Article

Post-Impact Stabilization during Lane Change Maneuver

Yeayoung Park [1], Juhui Gim [2],* and Changsun Ahn [1],*

1   School of Mechanical Engineering, Pusan National University, Busan 46241, Republic of Korea;
pyy3220@pusan.ac.kr
2   School of Electric, Electronic and Control Engineering, Changwon National University,
Changwon 51140, Republic of Korea
*   Correspondence: juhuigim@changwon.ac.kr (J.G.); sunahn@pusan.ac.kr (C.A.)

Abstract: This study addresses challenges in vehicle collisions, especially in non-front or non-rear impacts, causing rapid state changes and a loss of control. Electronic Stability Control (ESC) can stabilize a vehicle in minor impact cases, but it cannot effectively handle major collision cases. To overcome this, our research focuses on Post-Impact Stabilization Control (PISC). Existing PISC methods face issues like misidentifying collisions during cornering maneuvers due to assumptions of straight driving, rendering them ineffective for lane change accidents. Our study aims to design PISC specifically for cornering and lane change maneuvers, predicting collision forces solely from the ego vehicle's data, ensuring improved collision stability control. We employ the unscented Kalman filter to estimate collision forces and develop a sliding mode controller with an optimal force allocation algorithm to counter the disturbances caused by collisions and stabilize the vehicle. Rigorous validation through simulations and tests with a driving simulator demonstrates the feasibility of our proposed methodology in effectively stabilizing vehicles during collision accidents, particularly in lane change situations.

Keywords: collision force estimation; unscented Kalman filter; collision stabilization; post-impact stabilization control

1. Introduction

During vehicle collisions, especially in cases of non-front or non-rear collisions, the vehicle's state undergoes rapid changes, leading to the driver's loss of control, and the vehicle easily slips or spins. Currently, Electronic Stability Control (ESC) serves as a control system that assists the driver in maintaining vehicle stability during aggressive driving. However, ESC may not be suitable for handling major collisions since it does not account for the existence of external forces. While ESC can address minor collisions, it is not ideal for use in significant collisions. To address this issue, research is underway on a control system called Post-Impact Stabilization Control (PISC), which aims to stabilize a vehicle's state after a collision.

PISC is being studied in several forms. The first approach involves an activated controller with collision detection using pure signal processing of sensor measurements [1–4]. The second approach estimates collision forces resulting from inter-vehicle collisions to detect the occurrence of collisions, and it utilizes these collision forces in the control system [5–10]. Methods assuming the vehicle states of counterpart vehicles are available. The final approach involves assuming prior knowledge of collision severity and collision occurrence, and designing the system to operate without discerning collision occurrence [11–19].

In the first method, which is based on the vehicle's state for collision detection, collisions are identified when certain threshold values, such as the derivative of the longitudinal velocity or lateral velocity of the vehicle, are exceeded. This approach has the advantage of easily designing collision detection using only the sensor signal itself. However, it may mistakenly recognize a collision when the vehicle does not collide but exhibits abrupt

vehicle maneuvers beyond the threshold value. For example, situations like tight lane changes or sharp cornering might be incorrectly interpreted as collisions. For this reason, this method is valid only for straight driving situations.

The second approach, estimating collision forces between vehicles, resolves the issues of the first method by estimating collision forces. However, conventional research on estimating inter-vehicle collision forces faces challenges such as the need for vehicle-to-vehicle (V2V) communication to acquire the state information of other vehicles involved in the collision or the assumption of collision force shapes for estimation.

The final approach, assuming or not identifying collision occurrence, reduces the difficulty in designing a controller since collisions are not directly detected. While not inherently flawed, this method lacks the capability to incorporate evolving changes in the vehicle state influencing collision dynamics into the controller's predictions. Additionally, it requires a separate determination of collision situations, presenting a drawback. For instance, a separate collision detection system or an assumption of already detected collisions is necessary to use the controller.

Therefore, in this study, our goal is to design a PISC that can be applied in cornering or lane change scenarios without the necessity of the assumption of straight driving and the need for information about other vehicles' states. This is achieved by predicting collision forces using only information from the ego vehicle. To do this, we use the unscented Kalman filter (UKF) to estimate collision forces and develop a sliding mode controller with an optimal force allocation algorithm to counter the disturbances caused by collisions and to stabilize the vehicle.

In previous research, Model Predictive Control (MPC) has been extensively utilized as a controller [8,9,11,12,15], proving to be an effective method for post-collision vehicle state stabilization by predicting the vehicle's state after a collision. MPC requires future information for its implementation. In this context, future information refers to the future impact force and driver's future steering input. Therefore, in prior research, vehicle collision models were predefined to predict the future impact force. For the knowledge on the driver's future steering input, MPC assumes a fixed steering angle, which can be valid in straight driving cases. However, predefined collision models are too simple for the prediction of complex collision forces. Furthermore, the assumption of a fixed steering angle is not valid when the vehicle lateral maneuver exists or when the driver actively reacts to the impact by rotating the steering wheel.

Additionally, research on PISC is also being conducted on the application of a sliding mode controller (SMC) [1,2,6,10,14]. SMC is a nonlinear control method that provides robust control against uncertainties and external disturbances in a system. This controller focuses on minimizing the error between the desired state and the current state of the system by forcing a set of states to converge to a specific surface known as the sliding mode surface. Unlike MPC, this controller effectively stabilizes the system without requiring future information and is robust in the presence of disturbances. Given that this matches the desired controller form pursued in this study, a PISC controller utilizing SMC is designed. However, incorporating constraints into the controller necessitates additional considerations. To address this, the allocation of forces acting on each tire is performed, taking into account constraints imposed on the controller actuators.

Therefore, the proposed PISC in this study consists of an estimator based on UKF for estimating collision forces during impact events and an SMC-based controller to stabilize the vehicle based on the estimated collision forces. Furthermore, to account for constraints, the optimal allocation is employed to determine the forces corresponding to each tire, and these forces are subsequently transmitted to actuators. This controller is applicable regardless of the driving scenario, providing an effective vehicle stabilization controller that considers the driver's intentions, even after a collision.

The subsequent sections of this paper are organized as follows: Section 2 outlines the collision force estimator based on UKF, focusing on the estimation of the collision lateral force and yaw momentum. In Section 3, we present the design of the SMC-based controller,

addressing both the stabilization of vehicle motion and the driver's driving ability. The validation of the proposed controller using CarSim and a driving simulator is detailed in Section 4. Lastly, Section 5 offers concluding remarks summarizing the key findings of this study.

2. Collision Force Estimator

2.1. Vehicle Model for Estimator Design

The estimator design incorporates a 3-degree-of-freedom (3-dof) vehicle model with collision forces, as illustrated in Figure 1. To accurately capture the vehicle's extreme motion following a collision, we formulated a nonlinear vehicle model that includes collision forces. The corresponding equation for the vehicle model is

$$
\begin{bmatrix} \dot{v}_x \\ \dot{v}_y \\ \dot{r} \end{bmatrix} = \begin{bmatrix} f_1\left(v_x, v_y, r, \delta_f\right) \\ f_2\left(v_x, v_y, r, \delta_f\right) \\ f_3\left(v_x, v_y, r, \delta_f\right) \end{bmatrix} + G \begin{bmatrix} F_{x,impact} \\ F_{y,impact} \\ M_{z,impact} \end{bmatrix},
\tag{1}
$$

with the following functions:

$$
\begin{aligned}
f_1 &= \frac{1}{m}\left(F_{xF}\left(v_y, r, \delta_f\right)\cos\left(\delta_f\right) + F_{xR}\left(v_y, r\right) + F_{yf}\left(v_y, r, \delta_f\right)\sin\left(\delta_f\right)\right) + v_y r, \\
f_2 &= \frac{1}{m}\left(F_{xF}\left(v_y, r, \delta_f\right)\sin\left(\delta_f\right) + F_{yF}\left(v_y, r, \delta_f\right)\cos\left(\delta_f\right) + F_{yR}\left(v_y, r\right)\right) - v_x r, \\
f_3 &= \frac{1}{I_{zz}}\left(a\left(F_{xF}\left(v_y, r, \delta_f\right)\sin\left(\delta_f\right) + F_{yF}\left(v_y, r, \delta_f\right)\cos\left(\delta_f\right)\right) - bF_{yR}\left(v_y, r\right)\right. \\
&\quad \left. + \frac{d}{2}\left(\left(F_{xFR} - F_{xFL}\right)\cos\left(\delta_f\right) + \left(F_{xRR} - F_{xRL}\right) + \left(F_{yFR} - F_{yFL}\right)\sin\left(\delta_f\right)\right)\right), \\
G &= \begin{bmatrix} \frac{1}{m} & 0 & 0 \\ 0 & \frac{1}{m} & 0 \\ 0 & 0 & \frac{1}{I_{zz}} \end{bmatrix},
\end{aligned}
$$

where v_x is the longitudinal velocity, v_y is the lateral velocity, r is the yaw rate, δ_f is the front steering angle, $F_{x,impact}$ is the collision force in the longitudinal direction, $F_{y,impact}$ is the collision force in the lateral direction, $M_{z,impact}$ is the collision yaw moment, m is the vehicle mass, F_x is the longitudinal tire force, F_y is the lateral tire force, I_{zz} is the yaw moment of inertia, a is the length of the front axle to the center of gravity, and b is the length of the rear axle to the center of gravity. Subscript F is the front tire, R is the rear tire, FL is the front left tire, FR is the front right tire, RL is the rear left tire, and RR is the rear right tire.
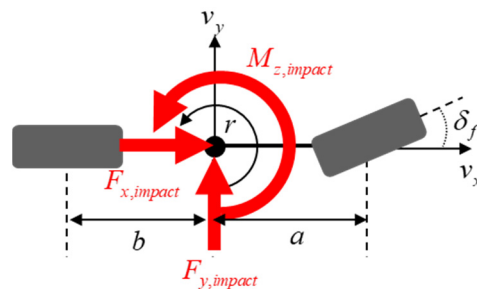

Figure 1. The 3-dof vehicle model considering collision force.

Given the necessity to account for the substantial lateral slip resulting from collision accidents, a basic linear tire model proves insufficient. To address this, the Magic Formula, as depicted in Figure 2, is employed to capture the essential nonlinear behavior. The total longitudinal and lateral tire forces, dependent on the longitudinal slip (kappa, κ) and lateral slip (alpha, α), are determined utilizing the approach detailed by Bakker et al. [20].
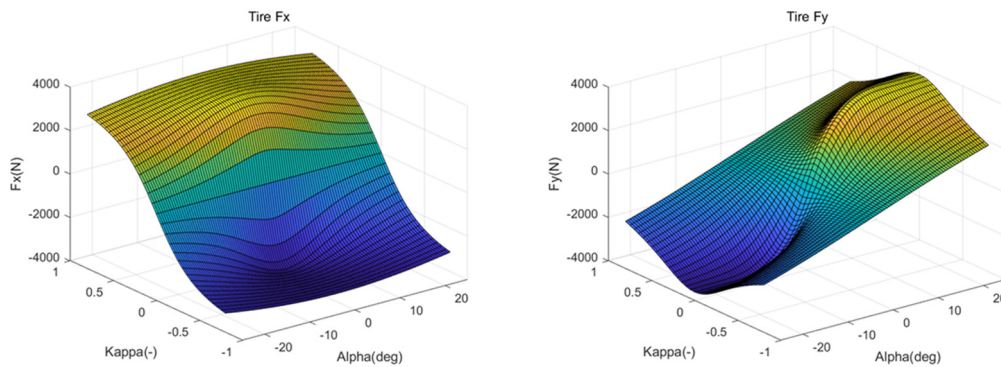
Figure 2. Nonlinear tire force model.

2.2. Collision Force Estimator

A disturbance observer has been developed within the Kalman filter framework to estimate the lateral collision force and collision momentum. The nonlinearity of the vehicle model renders a basic Kalman filter ineffective, necessitating the use of an extended Kalman filter (EKF) or unscented Kalman filter (UKF). In this scenario, employing EKF for collision estimation becomes problematic when the vehicle model's Jacobian matrix becomes singular—either at the maximum tire force or when it experiences minimal changes. Consequently, this paper opts for UKF.

We used unscented Kalman filter unbiased minimum-variance (UKF-UMV) [21] to design a disturbance observer. The measurements of UKF are the same with vehicle model states. A nonlinear discrete-time system considering unknown inputs can be expressed as follows:

$$x_k = f(x_{k-1}, u_k) + Gd_k + w_k \tag{2}$$

$$z_k = h(x_k, u_k) + v_k \tag{3}$$

where f is the nonlinear system model, h is the measurement model, G is the disturbance-to-state matrix, d_k is unknown inputs, w_k is the process noise, and v_k is the measurement noise.

The sigma points are designed by considering the state with mean x and covariance matrix P_{k-1}^+ as follows:

$$x^{(i)} = \overline{x} + \left(\sqrt{N_x P_{k-1}^+} \right)_i, i = 1, \ldots, N_x, \tag{4}$$

$$x^{(i+N_x)} = \overline{x} - \left(\sqrt{N_x P_{k-1}^+} \right)_i, i = N_x + 1, \ldots, 2N_x, \tag{5}$$

where N_x is the number of states. Each sigma point is transformed through the nonlinear model as follows:

$$\hat{x}_{\alpha,k}^{(i)} = f(x_{\alpha,k-1}^{(i)}, u_{k-1}). \tag{6}$$

The predicted state mean and covariance matrix are computed using

$$\hat{x}_k^- = \sum_i W^{(i)} \hat{x}_{\alpha,k}^{(i)}, \tag{7}$$

$$P_k^- = \sum_i W^{(i)} \left[\hat{x}_{\alpha,k}^{(i)} - \hat{x}_k^- \right] \left[\hat{x}_{\alpha,k}^{(i)} - \hat{x}_k^- \right]^T + Q_k, \tag{8}$$

where W is the weight of the sigma points, and Q_k is the covariance matrix of process noises. The new sigma points can be designed as follows:

$$\chi^{(i)} = \hat{x}_{\alpha,k}^{(i)} \pm \left(\sqrt{N_x P_k^-} \right), \tag{9}$$

and each sigma point is transformed through the measurement model as follows:

$$\hat{z}_{\alpha,k}^{(i)} = h\left(\chi^{(i)}, u_k\right),\tag{10}$$

The predicted measurement mean, innovation, and cross-covariance matrices are computed using

$$\hat{z}_k = \sum_i W^{(i)} \hat{z}_{\alpha,k}^{(i)},\tag{11}$$

$$S_k = \sum_i W^{(i)} \left[\hat{z}_{\alpha,k}^{(i)} - \hat{z}_k\right]\left[\hat{z}_{\alpha,k}^{(i)} - \hat{z}_k\right]^T + R_k,\tag{12}$$

$$P_{xz,k} = \sum_i W_i \left[\chi^{(i)} - \hat{x}_k^-\right]\left[\hat{z}_{\alpha,k}^{(i)} - \hat{z}_k\right]^T,\tag{13}$$

where R_k is the covariance matrix of measurement noises. The Kalman gain is given as

$$K_k = P_{xz,k}S_k^{-1},\tag{14}$$

and, by applying statistical linearization to the nonlinear observation equation, the nonlinear observation equation can be express as

$$z_k = H_k(x_k - \overline{x}_k) + \hat{z}_k + \varepsilon_k\tag{15}$$

where variable ε_k is the statistical linearization error. Matrix H_k is calculated using

$$H_k = P_{xz,k}^T \left(P_k^-\right)^{-1},\tag{16}$$

According to [21], the estimated unknown input is computed using

$$\hat{d}_k = M_k[z_k - \hat{z}_k],\tag{17}$$

where

$$M_k = \left[GH_k S_k^{-1} H_k^T G^T\right]^{-1} G^T H_k^T S_k^{-1},$$

The updated state and covariance matrix are shown as

$$\hat{x}_k^+ = \hat{x}_k^- + G\hat{d}_k + K_k\left[z_k - \hat{z}_k - H_k G\hat{d}_k\right],\tag{18}$$

$$P_k^+ = P_k^- - K_k H_k P_k^- + (G - K_k H_k G)\left(G^T H_k^T S_k^{-1} H_k G\right)^{-1}(G - K_k H_k G)^T\tag{19}$$

The foundation of UKF-UMV lies in the assumption that measurement errors arise from unknown disturbances, potentially diminishing the estimation accuracy when substantial discrepancies exist in the system model. This issue becomes particularly critical when applied to the estimation of states and disturbances during significant lateral maneuvers in vehicles. In these situations, both vehicle and tire models are influenced by numerous unaccounted factors. To address this inherent inaccuracy, an error-dependent adaptive gain [22–26] is introduced into the UKF-UMV formula. The error-dependent adaptive gain is designed based on the magnitude of the measurement error. This is motivated by the fact that the measurement error arising from collisions between vehicles is greater than the error from vehicle and tire models. Equation (17) is then modified as follows:

$$\hat{d}_k = M_k[z_k - \hat{z}_k]\rho_k\tag{20}$$

where ρ_k is an adaptive tuning parameter, and the adaptive rule is as follows:

$$\rho_k = g(e_k), e_k = \|E_k\|_2^2\tag{21}$$

$$E_k = \sum_i W^{(i)}[z_k - \hat{z}_k][z_k - \hat{z}_k]^T \tag{22}$$

where $g(e_k)$ is a modified saturation function to attenuate the effect of a too-large measurement error. As shown in Figure 3, before e_k becomes lower than e_{th}, the error-dependent adaptive gain is adjusted according to the following curve. Once e_k reaches e_{th}, a constant value is applied.
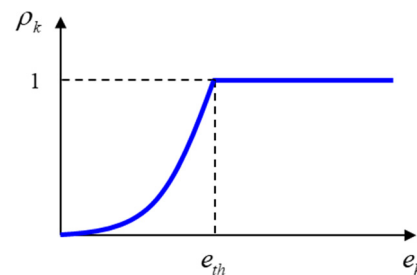

Figure 3. Modified saturation function (e_{th} is a tuning parameter).

2.3. Validation of Collision Force Estimator

To validate the collision force estimator, we utilized the vehicle dynamics program CarSim of Mechanical Simulation (ver. 2019.1). CarSim is software used for the analysis and simulation of vehicle dynamics. This program is employed to simulate various dynamic aspects of a vehicle to quantify and predict its motion. It can simulate the behavior of a vehicle under real driving conditions using different vehicle models and road conditions.

The validation process involved three distinct time trajectories of collision forces: a triangular shape, a half cycle of a sinusoidal curve, and the shape derived from actual collision force data obtained from crash tests conducted by the National Highway Traffic Safety Administration (NHTSA). The test maneuver was specifically designed to simulate a collision occurring during a single lane change, as illustrated in Figure 4.
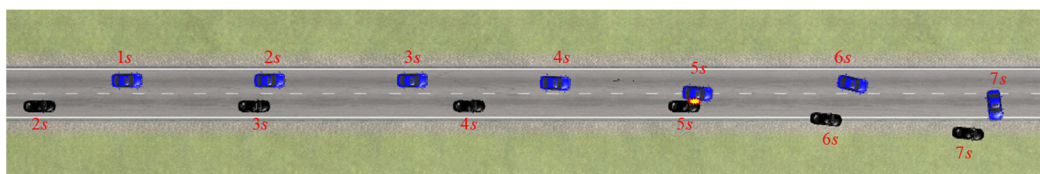

Figure 4. Test scenario used to validate collision force estimator. (blue: target vehicle, black: bullet vehicle).

The validation results are depicted in Figures 5–7. In these figures, (a) illustrates the outcomes without the error-dependent adaptive gain, whereas (b) illustrates the results with the adaptive gain applied. Figure 5 is the result with the triangular-shaped collision force. In Figure 5a, significant estimation errors are observed not only after the collision but also before the collision. This indicates that UKF-UMV intentionally incorporates vehicle and tire errors into the force when estimating external forces. However, the results with the error-dependent adaptive gain in Figure 5b notably eliminate pre- and post-collision errors. This outcome is also evident in Figure 6, where the collision force profile is altered to half a cycle of a sinusoidal curve. Additionally, the simulation results in Figure 7, incorporating real collision profiles alongside artificially induced collisions, confirm the disappearance of errors both before and after the collision depending on the utilization of adaptive gain. The utilization of adaptive gain clearly reduces the misestimated disturbance values. However, it is important to note that the error-dependent adaptive gain introduces a slight delay in the tracking of the actual values at the moment of collision.
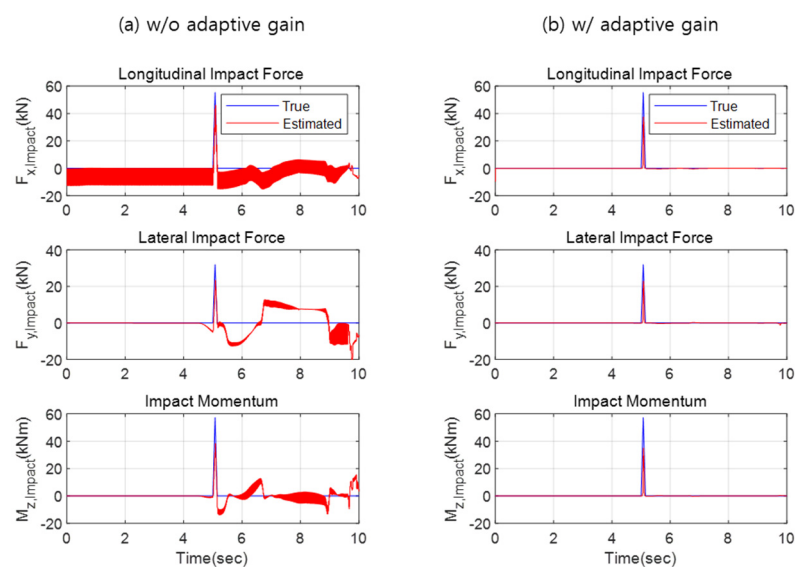
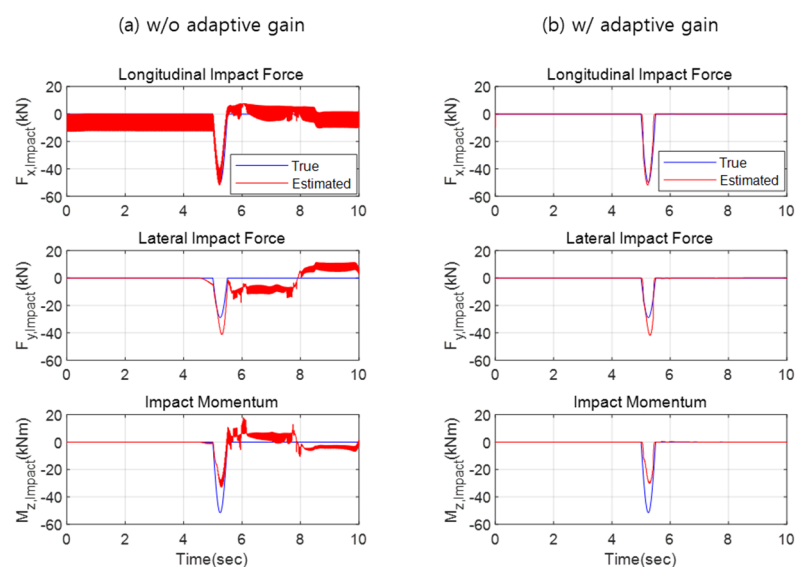**Figure 5.** Validation result—triangular form.

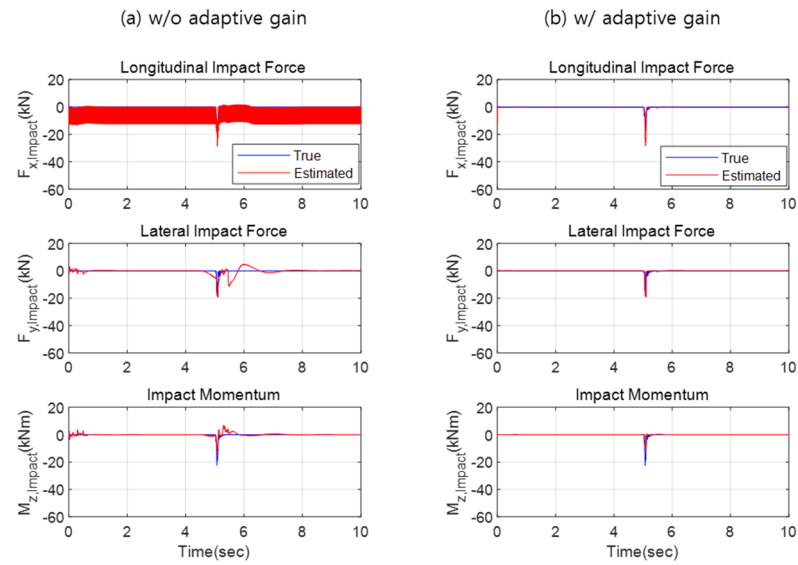**Figure 6.** Validation result—sine wave form.

Figure 7. Validation result—actual collision wave form (NHTSA crash no. 04667).

3. Post-Impact Stabilization Controller

We consider a vehicle equipped with an active front steer (AFS) system, rear wheel steer (RWS) system, and brake control system such as ESC, as shown in Figure 8a. Therefore, the available control variables for PISC are composed of four brake pressure values, an angle value for AFS, and another angle value for RWS.
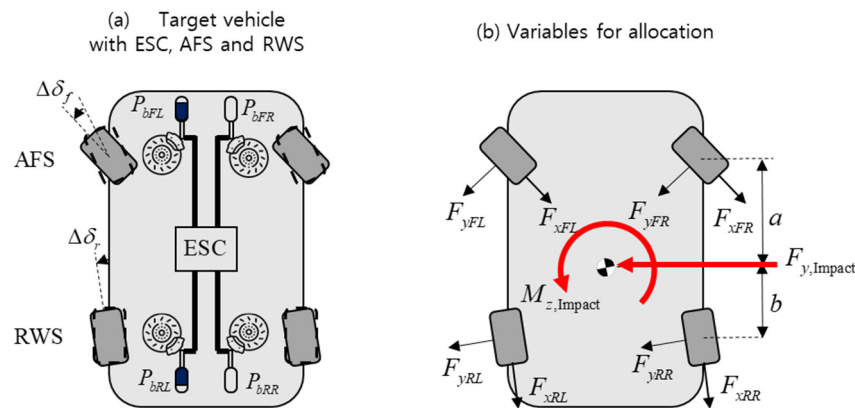

Figure 8. Target plant for PISC and corresponding forces.

The post-impact stabilization controller consists of several components: a collision force estimator, a controller activation trigger, a high-level controller, a low-level controller, and an actuator controller, as depicted in Figure 9. The controller activation trigger determines the activation based on the impact force's strength. The high-level controller, designed using sliding mode control theory, computes the total lateral force and momentum relative to the vehicle's center of mass, ensuring vehicle stability. The low-level controller allocates these forces into longitudinal and lateral forces for individual tires. Finally, the actuator controller calculates the required steering angle and brake pressure to generate the specified tire forces.
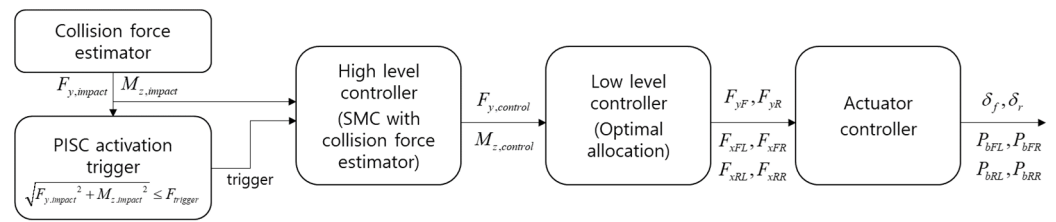
Figure 9. Structure of proposed post-impact stabilization controller.

3.1. High-Level Controller (Sliding Mode Control)

The high-level controller computes the total lateral force and momentum to stabilize the vehicle's motion and meet the driver's control desire. Sliding mode control (SMC) was employed as the controller design method due to its effectiveness in achieving the desired performance in the presence of disturbances. The control model utilized is a 2-degree-of-freedom (2-dof) nonlinear vehicle model, encompassing both disturbance inputs and control inputs, as follows:

$$
\begin{aligned}
M(\dot{v}_y + v_x r) = \ & (F_{xFL} + F_{xFR}) \sin \delta_f + (F_{yFL} + F_{yFR}) \cos \delta_f \\
& + (F_{xRL} + F_{xRR}) \sin \delta_r + (F_{yRL} + F_{yRR}) \cos \delta_r \\
& + F_{y,impact} + F_{y,control},
\end{aligned}
\tag{23}
$$

$$
\begin{aligned}
I_{zz}\dot{r} = \ & a(F_{xFL} + F_{xFR}) \sin \delta_f + a(F_{yFL} + F_{yFR}) \cos \delta_f \\
& - b(F_{xRL} + F_{xRR}) \sin \delta_r - b(F_{yRL} + F_{yRR}) \cos \delta_r \\
& + \frac{d}{2} \Big[(F_{xFR} - F_{xFL}) \cos \delta_f + (F_{xRR} - F_{xRL}) \cos \delta_r \\
& + (F_{yFL} - F_{yFR}) \sin \delta_f + (F_{yRL} - F_{yRR}) \sin \delta_r \Big] \\
& + M_{z,impact} + M_{z,control},
\end{aligned}
\tag{24}
$$

where δ_r is the rear steering angle, d is the vehicle width, $F_{y,input}$ and $M_{z,input}$ are the estimated lateral impact force and impact momentum, and $F_{y,control}$ and $M_{z,control}$ are the control lateral force and yaw momentum.

The primary objective of PISC is to stabilize both the lateral and yaw motion of the vehicle. To achieve this goal, the lateral velocity and yaw rate are chosen as the states for SMC. The lateral force and yaw momentum serve as the control inputs for stabilization. Two distinct SMC surfaces are established: one is designed to stabilize the lateral motion, while the other is tailored to fulfill the driver's intended yaw rate. The equations defining the states, control inputs, and sliding surfaces are provided below:

$$
\begin{cases} x_1 = v_y \\ x_2 = r \end{cases} , \quad \begin{cases} u_1 = F_{y,control} \\ u_2 = M_{z,control} \end{cases}
\tag{25}
$$

$$
\begin{cases} S_1 = x_1, & \dot{S}_1 = -k_1 S_1 \\ S_2 = x_2 - r_{des}, & \dot{S}_2 = -k_2 S_2 \end{cases}
\tag{26}
$$

where k_1 and k_2 are the positive and mean convergence rates. The driver's desired yaw rate, r_{des}, can be computed once the wheel base, L, and the understeer gradient, K_{us}, are given as follows:

$$
r_{des} = \frac{v_x}{L + K_{us} v_x^2} \delta_f.
\tag{27}
$$

By implementing the following control law, the states approach the sliding surface:

$$
\begin{aligned}
u_{1,d} = \ & M(v_x r - k_1 v_y) - ((F_{xFL} + F_{xFR}) \sin \delta_f + (F_{yFL} + F_{yFR}) \cos \delta_f \\
& + (F_{xRL} + F_{xRR}) \sin \delta_r + (F_{yRL} + F_{yRR}) \cos \delta_r) - F_{y,impact}
\end{aligned}
\tag{28}
$$

$$
\begin{aligned}
u_{2,d} = \; & I_{zz}\left(\dot{r}_{des} - k_2(r - r_{des})\right) - \left(a(F_{xFL} + F_{xFR})\sin\delta_f + a\left(F_{yFL} + F_{yFR}\right)\cos\delta_f\right. \\
& - b(F_{xRL} + F_{xRR})\sin\delta_r - b\left(F_{yRL} + F_{yRR}\right)\cos\delta_r + \tfrac{d}{2}\left[(F_{xFR} - F_{xFL})\cos\delta_f\right. \\
& \left.\left. + (F_{xRR} - F_{xRL})\cos\delta_r + \left(F_{yFL} - F_{yFR}\right)\sin\delta_f + \left(F_{yRL} - F_{yRR}\right)\sin\delta_r\right]\right) - M_{z,impact}
\end{aligned}
\tag{29}
$$

where $u_{1,d}$ and $u_{2,d}$ are the desired control inputs.

3.2. Low-Level Controller (Optimal Allocation)

The total lateral force and yaw momentum computed in the high-level controller should be allocated to each tire. We design an optimal allocation problem so that the tires are far from the force saturation state as follows:

$$
\min_q J(q),
\tag{30}
$$

subject to

$$
Hq = C,
\tag{31}
$$

$$
\begin{aligned}
0 \leq F_{x,ij} \leq F_{x,ij,\lim,h}, \\
F_{y,ij,\lim,l} \leq F_{y,ij} \leq F_{y,ij,\lim,h}.
\end{aligned}
\tag{32}
$$

The corresponding symbols are defined as follows:

$$
q = \begin{bmatrix} F_{yF} & F_{yR} & F_{xFL} & F_{xFR} & F_{xRL} & F_{xRR} & F_{y,ext} & M_{z,ext} \end{bmatrix}^T,
$$

$$
\begin{aligned}
J &= q^T W q \\
&= \frac{\rho_1 F_{yF}^2 + \rho_3 F_{xFL}^2}{(\mu F_{zFL})^2} + \frac{\rho_1 F_{yF}^2 + \rho_4 F_{xFR}^2}{(\mu F_{zFR})^2} + \frac{\rho_2 F_{yR}^2 + \rho_5 F_{xRL}^2}{(\mu F_{zRL})^2} + \frac{\rho_2 F_{yR}^2 + \rho_6 F_{xRR}^2}{(\mu F_{zRR})^2} \\
&\quad + \rho_7 F_{y,ext}^2 + \rho_8 M_{z,ext}^2,
\end{aligned}
$$

$$
W = diag\begin{bmatrix} \frac{1}{\xi_1^2} + \frac{1}{\xi_2^2} & \frac{1}{\xi_3^2} + \frac{1}{\xi_4^2} & \frac{1}{\xi_1^2} & \frac{1}{\xi_2^2} & \frac{1}{\xi_3^2} & \frac{1}{\xi_4^2} & 1 & 1 \end{bmatrix}\rho
$$

$$
\rho = \begin{bmatrix} \rho_1 & \rho_2 & \rho_3 & \rho_4 & \rho_5 & \rho_6 & \rho_7 & \rho_8 \end{bmatrix}^T
$$

$$
\xi_1 = \mu F_{zFL}, \; \xi_2 = \mu F_{zFR}, \; \xi_3 = \mu F_{zRL}, \; \xi_4 = \mu F_{zRR},
$$

$$
H = \begin{bmatrix} a_{11} & a_{12} & a_{13} & a_{14} & a_{15} & a_{16} & 1 & 0 \\ a_{21} & a_{22} & a_{23} & a_{24} & a_{25} & a_{26} & 0 & 1 \end{bmatrix}, \; C = \begin{bmatrix} F_{y,control} & M_{b,control} \end{bmatrix}^T
$$

$$
a_{11} = 2\cos\delta_f, \; a_{12} = 2\cos\delta_r, \; a_{13} = -\sin\delta_f, \; a_{14} = -\sin\delta_f, \; a_{15} = -\sin\delta_r, \; a_{16} = -\sin\delta_r,
$$
$$
a_{21} = 2a\cos\delta_f, \; a_{22} = -2b\cos\delta_r, \; a_{23} = -a\sin\delta_f + \tfrac{d}{2}\cos\delta_f,
$$
$$
a_{24} = -a\sin\delta_f - \tfrac{d}{2}\cos\delta_f, \; a_{25} = b\sin\delta_r + \tfrac{d}{2}\cos\delta_r, \; a_{26} = b\sin\delta_r - \tfrac{d}{2}\cos\delta_r
$$

where ρ_i is the weight of the *i*th control input, and μ is the friction coefficient.

In Equation (30), cost function J represents the weighted sum of the tire utilization ratio and the deviation in the control input. The tire utilization ratio serves as an indicator of proximity to the saturation state, demonstrating how far the system is from reaching its limits. The deviation in the control input, denoted as $F_{y,ext}$ and $M_{z,ext}$, refers to dummy forces and moments introduced to uphold the equality constraint specified in Equation (31). This inclusion ensures compliance with the equality constraint, even if the available force and moment fail to meet it due to the need to avoid violating the inequality constraint. Consequently, the cost function is formulated to minimize both the overall tire saturation ratio and the extent to which the equality constraint is satisfied. The limit values within the

inequality constraint, as described in Equation (32), correspond to the maximum tire forces at a given instance.

3.3. Actuator Controller

Once the tire forces of each tire are determined in the optimal allocation algorithm, the corresponding actuator variables should be determined to generated the allocated forces. The brake pressure values of four brake disks are determined as follows:

$$P_{b,ij} = \frac{r_{tire}}{G_{fp}} F_{x,ij} \tag{33}$$

where r_{tire} is the effective wheel radius, and G_{jp} is the pressure to force gain.

The steering angle values of AFS and RWS must be determined to generate the commanded lateral force. The relationship between the steering angle and tire lateral forces is nonlinear. Calculating the steering angle for a given tire force is efficiently accomplished using a numerically efficient inversion method [27].

4. Validation

To validate the proposed methodology, two distinct tests were conducted. The first test involved a simulation using Carsim, a specialized vehicle dynamics simulation program. The second test was conducted on a driving simulator. To evaluate the control performance, we compared two algorithms: our proposed PISC algorithm (referred to as 'PISC Plus') and a benchmark controller that integrates ESC, AFS, and RWS based on SMC [28] (referred to as 'ESC+AFS+RWS'), which does not explicitly consider collision forces. The benchmark controller shares a similar structure with PISC Plus, as illustrated in Figures 9 and 10. The key differences lie in the presence of the collision force estimator and the criteria for control activation. The benchmark controller, ESC+AFS+RWS, becomes active when the measured yaw rate deviates from the desired yaw rate by a specified threshold.
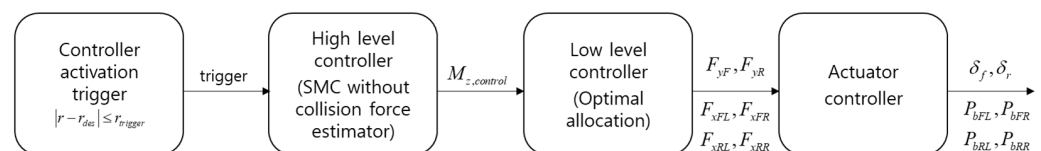
Figure 10. Structure of benchmark controller (ESC+AFS+RWS).

4.1. Validation with a Vehicle Driven by a Driver Model

In this set of validation tests, the test vehicle was a generic D-class Sedan equipped with AFS, RWS, and ESC. The test environment was designed as a highway with two lanes. The test maneuver was specifically designed to replicate a collision scenario during a single lane change, with the vehicle's velocity set to 80 km/h. The embedded driver model in CarSim controlled the target vehicle, executing path-following maneuvers with a 0.5 s lookahead setting. During the simulation, a bullet vehicle impacted the target vehicle while the target vehicle was performing the lane change. The collision point was located 0.4474 m behind the center of mass and 0.7750 m to the right of the center of mass, as illustrated in Figure 11.
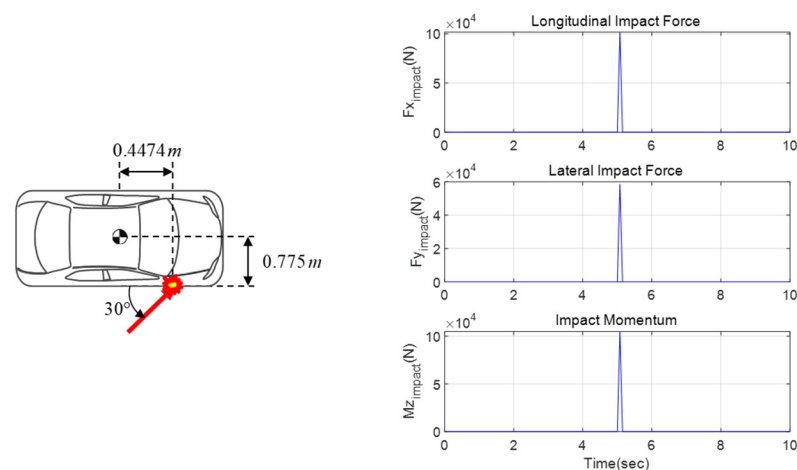
Figure 11. Impact position and impact force.

The vehicle motions and trajectories in three scenarios are depicted in Figure 12. The first case, indicated in blue, employed the PISC Plus algorithm. The second case, shown in red, involved the ESC + AFS + RWS algorithm. The third case, represented in green, had no control algorithm applied. The black vehicle represents the bullet vehicle. In these scenarios, only the PISC Plus algorithm ensured the stability of the target vehicle impacted by the bullet vehicle. In the other cases, all vehicles spun out of control.
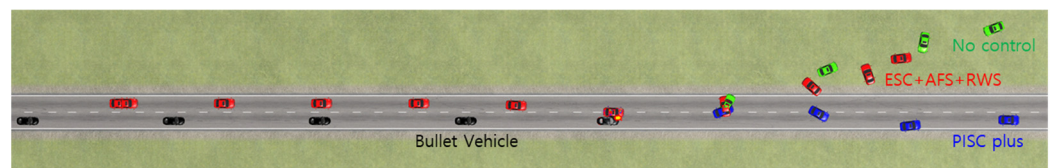
Figure 12. Vehicle motion and trajectories in three scenarios in simulation validation.

Figure 13 displays the corresponding signals from the simulation of the three different scenarios. The PISC Plus controller was activated immediately after the collision occurred thanks to the collision force detection algorithm. The reaction time of PISC Plus was 0.02 s, whereas that of the benchmark controller was 0.03 s. This difference can be attributed to the collision force estimator, which allows for earlier accident detection than signal-based detectors such as yaw-rate-based algorithms. Moreover, PISC Plus demonstrated the capability to incorporate not only state feedback but also disturbance feedback. As a result, it generated momentarily larger control inputs upon collision than the benchmark controller. This feature significantly contributes to vehicle state stabilization and enhances driving maneuver stability for the driver.

4.2. Validation with a Vehicle Driven by a Human Driver

We further validated the controller using a driving simulator, as illustrated in Figure 14. The test environment was the same as the simulation environment. The main difference was that the driver was a human not a model, which made the test more realistic. The human driver actively manipulated the steering wheel, acceleration pedal, and brake pedal to perform the lane change maneuver. Consequently, the vehicle trajectories and motions in the three scenarios leading up to the collision differed from those in the simulation validation. However, the impact's location and intensity remained consistent across the three scenarios and matched the simulation validation cases because the bullet vehicle adhered to a predetermined rule. As a result, the impact described in Figure 11 influenced the target vehicle as depicted.
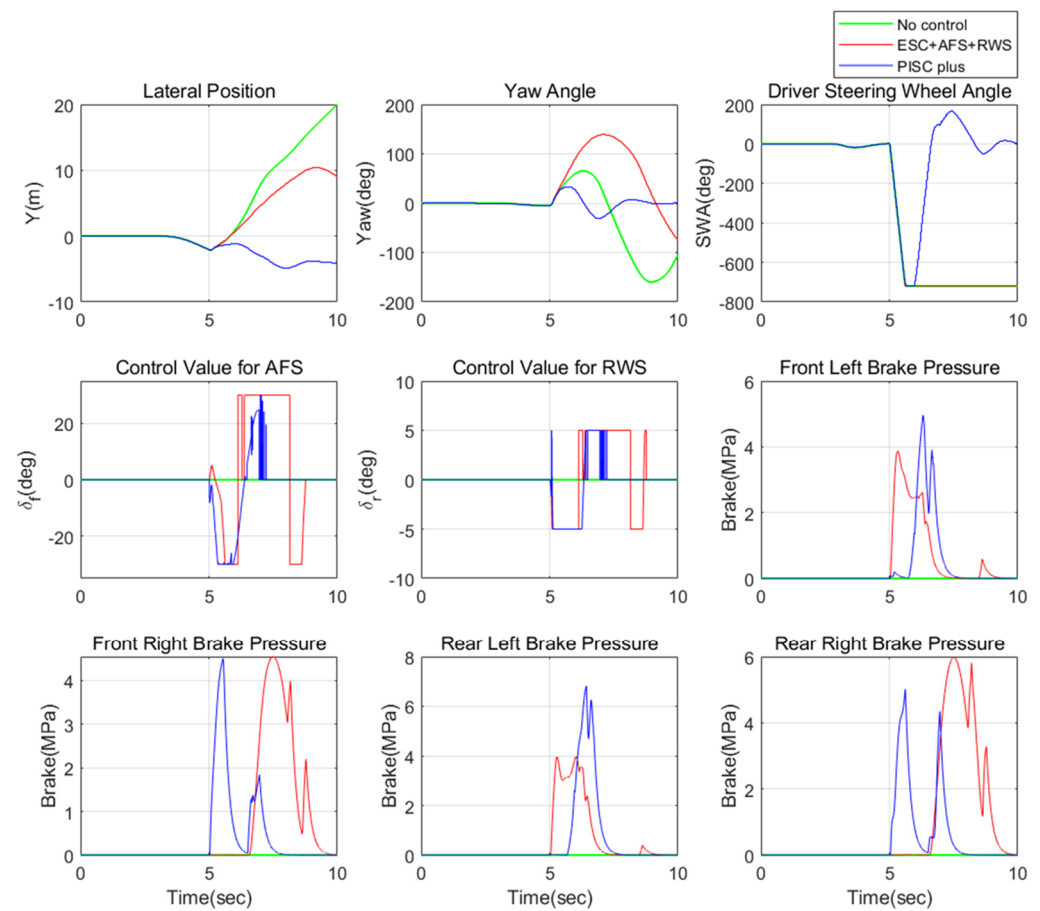
Figure 13. Vehicle states and control inputs of simulation validation.

Figure 14. Driving simulator.

The vehicle motions and trajectories in the three scenarios are illustrated in Figure 15. Similar to the findings from the simulation validation, only the PISC Plus algorithm ensured the stability of the target vehicle. Figure 16 displays the vehicle states and control inputs for PISC Plus and ESC + AFS + RWS. PISC Plus consistently outperformed the benchmark controller in these scenarios. The reaction time of PISC Plus was 0.02 s, whereas that of the benchmark controller was 0.04 s. Even considering the variation in the initial state of the vehicle for each case due to the driving, it could be observed that PISC Plus reacted more quickly. Despite the fact that the benchmark controller provided larger inputs after the collision, the vehicle failed to stabilize. This indicates that a quick response time has a

significant impact on post-collision vehicle stabilization. The test results confirm that the proposed algorithm performs as effectively as when a human driver is involved.
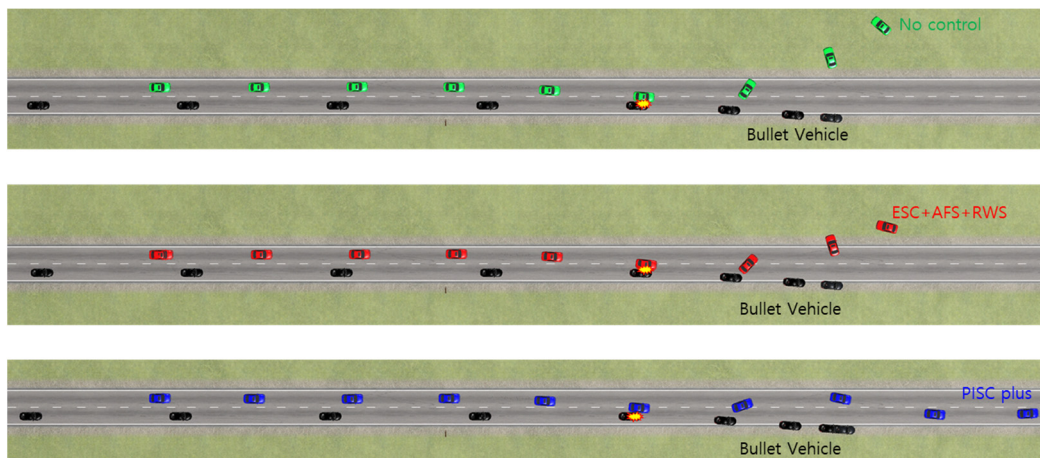

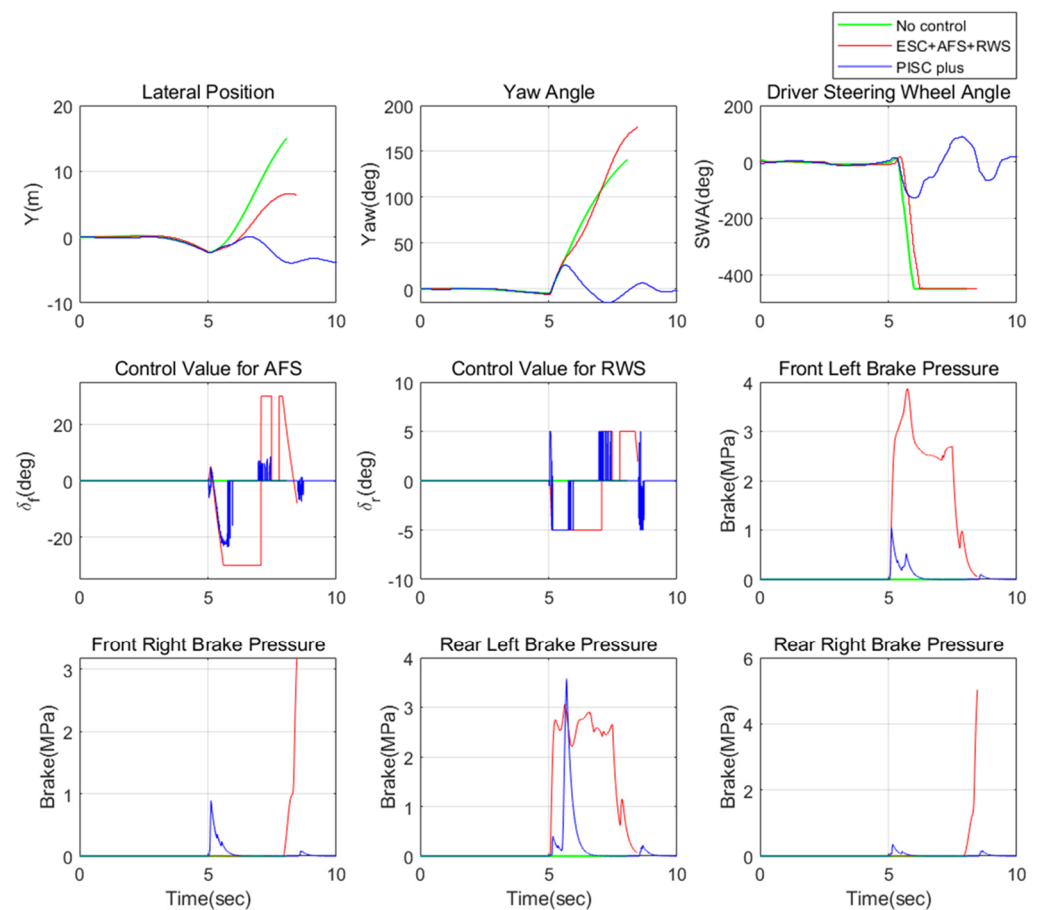**Figure 15.** Vehicle motions and trajectories in three scenarios in validation with driving simulator.

Figure 16. Vehicle states and control inputs of validation with driving simulator.

4.3. Rigorous Validation for Several Strengths, Impact Positions, and Impact Angles

The critical factors determining a controller's ability to stabilize a vehicle impacted by a bullet vehicle include the strength of the impact, the impact position, and the angle of impact. This is because the state of the vehicle after a collision is determined by these factors. When a very small impact is applied, most controllers can effectively stabilize the vehicle. But, as the collision force increases, the vehicle state undergoes rapid changes,

making vehicle stabilization challenging. Additionally, the difficulty of stabilization varies with the impact position and angle. Stabilization becomes easier when the collision angle aligns with the direction of the vehicle's center of gravity. To assess controller performance in post-impact stabilization operations, we can compare the maximum strength of impacts with which a controller can stabilize a vehicle.

Figure 17 displays the maximum allowable or stabilizable collision impulse concerning various sets of impact positions and angles. Through rigorous simulations, we can confidently assert that PISC Plus outperforms ESC + AFS + RWS. This finding demonstrates that PISC Plus significantly enhances vehicle stability after a collision accident in the majority of cases. This is because the collision force estimator in PISC Plus makes an excellent collision force estimation, providing a faster response and larger proactive inputs to the controller than ESC+AFS+RWS by conveying these values to the controller. Additionally, when considering the results in Sections 4.1 and 4.2 collectively, it implies that fast and substantial control inputs after a collision, as observed in post-collision vehicle attitude control, can be significant factors in stabilizing the vehicle state.
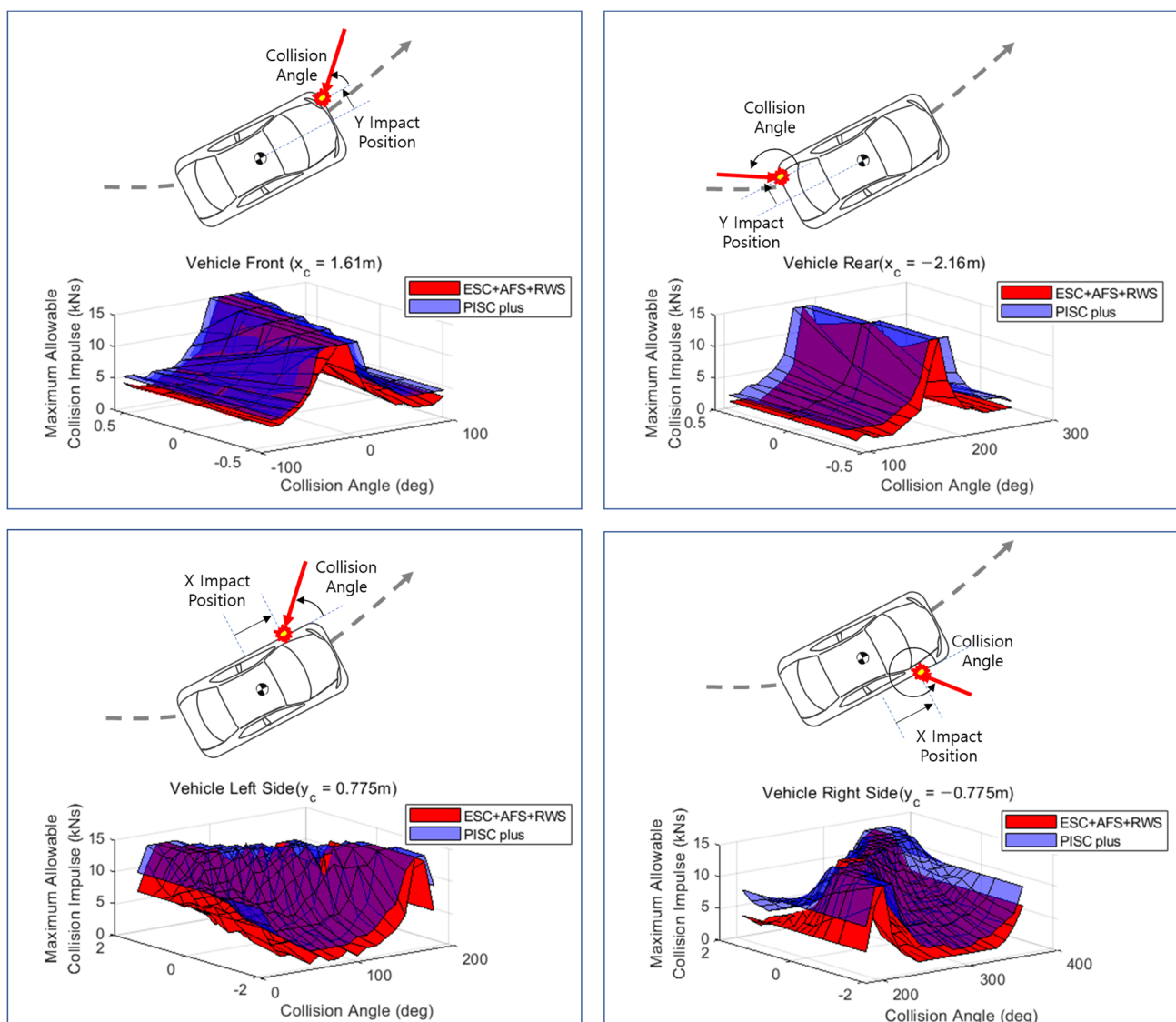

Figure 17. Maximum allowable collision impulse w.r.t. various sets of impact positions and angles.

5. Conclusions

In this study, we addressed the challenges of non-front or non-rear vehicle collisions by introducing advanced Post-Impact Stabilization Control (PISC Plus). The proposed control algorithm, predicting collision forces from the ego vehicle's data using the unscented Kalman filter, proved highly effective in stabilizing vehicles during complex maneuvers, particularly lane changes. Comprehensive simulations and driving simulator tests showcased PISC Plus's superiority over the benchmark ESC + AFS + RWS system. Whether with a driver model or a human driver, PISC Plus consistently outperformed the benchmark, ensuring stability, even in unexpected collision scenarios. Our results, validated across various strengths, impact positions, and angles, demonstrate PISC Plus's exceptional performance. By accurately anticipating and counteracting collision forces, our system significantly enhances vehicle stability after accidents, especially in dynamic scenarios like lane changes.

Further exploration into real-time implementation and integration with emerging autonomous driving technologies could enhance the proposed algorithm's applicability. Additionally, investigating adaptive algorithms capable of handling various vehicle types and collision scenarios will be crucial for broader industry adoption.

References

1. Zhou, J. *Active Safety Measures for Vehicles Involved in Light Vehicle-to-Vehicle Impacts*; University of Michigan: Ann Arbor, MI, USA, 2009.
2. Ao, D.; Hua, X.; Yu, G.; Guo, D.; Jia, Z. Robust Active Post-Impact Motion Control for Restraining a Second Crash. In Proceedings of the 2020 IEEE 16th International Conference on Automation Science and Engineering (CASE), Hong Kong, China, 20–21 August 2020.
3. Li, Z.; Gao, C.; Zhu, Z.; Jia, Z. Post-Impact Control to Mitigate the Secondary Collision by Combining LQR with Feed-Forward Control. In Proceedings of the 2022 International Conference on Advanced Robotics and Mechatronics (ICARM), Guilin, China, 9–11 July 2022.
4. Hou, X.; Gan, M.; Zhang, J.; Zhao, S.; Ji, Y. Secondary crash mitigation controller after rear-end collisions using reinforcement learning. *Adv. Eng. Inform.* **2023**, *58*, 102176. [CrossRef]
5. Parseh, M.; Nybacka, M.; Asplund, F. Motion planning for autonomous vehicles with the inclusion of post-impact motions for minimising collision risk. *Veh. Syst. Dyn.* **2023**, *61*, 1707–1733. [CrossRef]
6. Kim, B.-j.; Peng, H. Collision Strength Estimation and Preemptive Steering Control for Post-Impact Vehicle Motion Control. In Proceedings of the 12th International Symposium on Advanced Vehicle Control, Tokyo, Japan, 22–26 September 2014.
7. Zhou, J.; Peng, H.; Lu, J. Collision model for vehicle motion prediction after light impacts. *Veh. Syst. Dyn.* **2008**, *46*, 3–15. [CrossRef]
8. Cao, M.; Hu, C.; Wang, R.; Wang, J.; Chen, N. Compensatory model predictive control for post-impact trajectory tracking via active front steering and differential torque vectoring. *Proc. Inst. Mech. Eng. Part D J. Automob. Eng.* **2021**, *235*, 903–919. [CrossRef]
9. Wang, C.; Wang, Z.; Zhang, Z.; Liu, J.; Li, W.; Wu, Y.; Li, X.; Yu, H.; Cao, D. Integrated post-impact planning and active safety control for autonomous vehicles. *IEEE Trans. Intell. Veh.* **2023**, *8*, 23238782. [CrossRef]
10. Ao, D.; Li, J.; Zhang, L.; Hong, J. Advanced post-impact safety and stability control for electric vehicles. *IET Intell. Transp. Syst.* **2022**, *16*, 1753–1767. [CrossRef]
11. Zheng, Y.; Shyrokau, B. A Real-Time Nonlinear MPC for Extreme Lateral Stabilization of Passenger Vehicles. In Proceedings of the 2019 IEEE International Conference on Mechatronics (ICM), Ilmenau, Germany, 18–20 March 2019.
12. Funke, J.; Brown, M.; Erlien, S.M.; Gerdes, J.C. Collision avoidance and stabilization for autonomous vehicles in emergency scenarios. *IEEE Trans. Control Syst. Technol.* **2016**, *25*, 1204–1216. [CrossRef]

13. Yang, D.; Jacobson, B.; Jonasson, M.; Gordon, T. Minimizing vehicle post impact path lateral deviation using optimized braking and steering sequences. *Int. J. Automot. Technol.* **2014**, *15*, 7–17. [CrossRef]

14. Wang, C.; Yu, H.; Zhang, L.; Wang, Z.; Wang, Q.; Cao, D. Post-Impact Stability Control for Four-Wheel-Independently-Actuated Electric Vehicles. In Proceedings of the 2020 Chinese Automation Congress (CAC), Shanghai, China, 6–8 November 2020.

15. Nigicser, D.; Valerio, T.; Mårtensson, J.; Mustafa, A.A.; da Silva, E.S. Predictive Vehicle Motion Control for Post-Crash Scenarios. In Proceedings of the 14th International Symposium on Advanced Vehicle Control, Beijing, China, 16–20 July 2018.

16. Yin, Y.; Li, S.E.; Li, K.; Yang, J.; Ma, F. Self-learning drift control of automated vehicles beyond handling limit after rear-end collision. *Transp. Saf. Environ.* **2020**, *2*, 97–105.

17. Delves, P.S. Simulation Study Investigating the Novel Use of Drive Torque Vectoring for Dynamic Post-Impact Vehicle Control. Ph.D. Thesis, Manchester Metropolitan University, Manchester, UK, 2015.

18. Chakraborty, I.; Tsiotras, P.; Diaz, R.S. Time-Optimal Vehicle Posture Control to Mitigate Unavoidable Collisions using Conventional Control Inputs. In Proceedings of the 2013 American Control Conference, Washington, DC, USA, 17–19 June 2013.

19. Wang, C.; Wang, Z.; Zhang, L.; Yu, H.; Cao, D. Post-impact motion planning and tracking control for autonomous vehicles. *Chin. J. Mech. Eng.* **2022**, *35*, 54.

20. Bakker, E.; Pacejka, H.B.; Lidner, L. A new tire model with an application in vehicle dynamics studies. *SAE Trans.* **1989**, *98*, 101–113.

21. Zheng, Z.; Zhao, J.; Mili, L.; Liu, Z.; Wang, S. Unscented Kalman filter-based unbiased minimum-variance estimation for nonlinear systems with unknown inputs. *IEEE Signal Process. Lett.* **2019**, *26*, 1162–1166. [CrossRef]

22. Zhang, Y.; Li, M.; Zhang, Y.; Hu, Z.; Sun, Q.; Lu, B. An enhanced adaptive unscented kalman filter for vehicle state estimation. *IEEE Trans. Instrum. Meas.* **2022**, *71*, 6502412. [CrossRef]

23. Hu, G.; Gao, B.; Zhong, Y.; Ni, L.; Gu, C. Robust unscented Kalman filtering with measurement error detection for tightly coupled INS/GNSS integration in hypersonic vehicle navigation. *IEEE Access* **2019**, *7*, 151409–151421. [CrossRef]

24. Vahidi, A.; Stefanopoulou, A.; Peng, H. Recursive least squares with forgetting for online estimation of vehicle mass and road grade: Theory and experiments. *Veh. Syst. Dyn.* **2005**, *43*, 31–55. [CrossRef]

25. Geng, Y.; Wang, J. Adaptive estimation of multiple fading factors in Kalman filter for navigation applications. *GPS Solut.* **2008**, *12*, 273–279. [CrossRef]

26. Kang, C.H.; Park, C.G.; Song, J.W. An adaptive complementary Kalman filter using fuzzy logic for a hybrid head tracker system. *IEEE Trans. Instrum. Meas.* **2016**, *65*, 2163–2173. [CrossRef]

27. Kang, B.; Ahn, C. Direct tire force generation algorithm based on non-iterative nonlinear inverse tire model. *Int. J. Automot. Technol.* **2017**, *18*, 983–992. [CrossRef]

28. Yim, S. Coordinated control with electronic stability control and active steering devices. *J. Mech. Sci. Technol.* **2015**, *29*, 5409–5416. [CrossRef]